The Cryosphere Discuss., 5, 1887–1920, 2011
www.the-cryosphere-discuss.net/5/1887/2011/
doi:10.5194/tcd-5-1887-2011

The Cryosphere Discussions

The impact of a seasonally ice free Arctic Ocean on the climate and surface mass balance of Svalbard

J. J. Day[1,2], **J. L. Bamber**[1], **P. J. Valdes**[1], **and J. Kohler**[3]

[1]School of Geographical Sciences, University of Bristol, Bristol, UK
[2]RIGC/JAMSTEC, Yokohama Institute for Earth Sciences, Yokohama, Japan
[3]Norsk Polarinstitutt, Polar Environment Centre, Tromsø, Norway

Received: 24 June 2011 – Accepted: 8 July 2011 – Published: 18 July 2011

Correspondence to: J. J. Day (jday@jamstec.go.jp)

Published by Copernicus Publications on behalf of the European Geosciences Union.

Abstract

General circulation models (GCMs) predict a rapid decrease in Arctic sea ice extent in the 21st century. The decline of September sea ice is expected to continue until the Arctic Ocean is seasonally ice free, leading to a much perturbed Arctic climate with large changes in surface energy flux. Svalbard, located on the present day sea ice edge, contains many low lying ice caps and glaciers which are extremely sensitive to changes in climate. Records of past accumulation indicate that the surface mass balance (SMB) of Svalbard is also sensitive to changes in the position of the sea ice edge.

To investigate the impact of 21st Century sea ice decline on the climate and surface mass balance of Svalbard a high resolution (25 km) regional climate model (RCM) was forced with a repeating cycle of sea surface temperatures (SSTs) and sea ice conditions for the periods 1961–1990 and 2061–2090. By prescribing 20th Century SSTs and 21st Century sea ice for one simulation, the impact of sea ice decline is isolated. This study shows that the coupled impact of sea ice decline and SST increase results in a decrease in SMB, whereas the impact of sea ice decline alone causes an increase in SMB of similar magnitude.

1 Introduction

Worldwide, observations of glaciers show an increasingly negative mass balance in recent years (Arendt et al., 2002; Kaser et al., 2006). Despite the fact that only 0.5 % of the Earth's terrestrial cryosphere consists of small glaciers and ice caps outside the ice sheets (Antarctica and Greenland), the smaller ice masses in the Arctic are thought to be a major contribution to this negative balance (Meier et al., 2007). The contribution from the Arctic is estimated to have increased from 0.27 mm a^{-1} sea level equivalent (SLE) 1961–1992 to 0.64 mm a^{-1} in 1993–2006 (Dyurgerov et al., 2010). Svalbard contributes significantly to this total, with estimates ranging from 0.013 to 0.026 mm a^{-1} SLE (Moholdt et al., 2010; Nuth et al., 2010; Wouters et al., 2008).

TCD
5, 1887–1920, 2011

Satellite monitoring since the late 1970s has shown that total Arctic sea ice extent has been declining, and at an accelerating rate since the 1990s (Serreze et al., 2007). The sea ice decline lies outside of the standard deviation of the model ensemble of projected decline included in the Intergovernmental Panel on Climate Change (IPCC) 4th Assessment Report (AR4) (Stroeve et al., 2007). Arctic sea ice retreat is thought to provide a major contribution to the positive trend in lower tropospheric Arctic temperature, which is amplified with respect to the global mean (Serreze et al., 2009). The decline in sea ice is expected to continue until the Arctic is seasonally ice-free at some point in the 21st Century (Boé et al., 2009; Wang and Overland, 2009).

Sea ice extent around Svalbard has been decreasing since the mid-1800s (Divine and Dick, 2006), concurrent with a general increase in temperatures (Nordli and Kohler, 2004). Accordingly, sea ice extent is thought to impact Svalbard glaciers, given their proximity to the ocean. Over the last 400 years the $\delta^{18}O$ record on the Austfonna ice cap correlates closely to the sea ice extent (Isaksson et al., 2005a,b) (location shown in Fig. 1). Anomalous increases of 35 % in accumulation rate on Austfonna between 1996–2002, were associated with changes in perennial ice cover around Nordaustlandet (Bamber et al., 2004; Raper et al., 2005). However, neither observations nor proxy reconstructions of SMB exist for past periods of low sea ice comparable to those expected in the 21st Century.

This study investigates what impact a seasonally ice free Arctic Ocean will have on the climate and surface mass balance (SMB) of Svalbard using a regional climate model (RCM). Atmospheric GCMs (AGCMs) are useful for investigating the impact of sea ice decline since they enable the use of experimental surface forcing, such as driving the surface boundary with present day SSTs and late 21st Century sea ice concentrations to isolate separate factors of change (Stein and Alpert, 1993). Deser et al. (2010) forced an AGCM with 1980–1999 SSTs and 2080–2099 sea ice conditions, and found that the response to the surface energy budget was largest in winter and smallest in summer and accounts for most of the seasonal, spatial and vertical structure of high latitude warming in coupled simulations used to provide the sea ice. Singarayer

TCD
5, 1887–1920, 2011

et al. (2006) suggest that some areas of Arctic land ice may even undergo net increase in accumulation due to sea ice decline.

Due to its relatively small size, Svalbard is not even represented as a land surface in many low resolution GCMs. Such GCMs are therefore not ideal for modelling climate changes (e.g. Hanssen-Bauer and Førland, 2001), arguing for the use of statistical and dynamical downscaling methods. While statistical methods add value to GCM-derived estimates of climate change, many methods are not physically based and some are limited to estimating change in regions in which there are existing observations (Fowler et al., 2007).

Here, we use a 25 km RCM to dynamically downscale AGCM scenarios. At this resolution, the RCM resolves the essential topography required to model circulation in the region. The use of RCMs represents a significant increase in model complexity compared to statistical downscaling studies in this region (e.g. Benestad et al., 2002; Rye et al., 2010).

A recent regional modelling study concluded that under the special report on emission scenarios (SRES) B2 emissions scenario (Nakicenovic and Swart, 2000), Svalbard is expected to experience an annual temperature increase of 3°C in the south west and 8°C in the north east from 1961–1990 to 2071–2100 with winter showing larger changes than summer. Annual precipitation is expected to increase by 10 % in the south west and 40 % in the north east over the same period (Førland et al., 2009). Førland et al. (2009), use the 25 km NorACIA-RCM version of HIRHAM over Svalbard forced with boundary conditions from the global Bergen Climate Model (BCM).

This study builds on this work of Førland et al. (2009) by incorporating an explicit investigation of the relative importance of sea ice decline on Svalbard's future climate and looking at the impact of future climate change on Svalbard's glacial SMB. It is the first regional impact study to investigate the climatic impact of sea ice decline using an RCM.

TCD
5, 1887–1920, 2011

The paper is set out as follows; in Sect. 2, we discuss the model set-up and justify the multiple nesting of RCMs. Section 3 describes the validation of the RCM with the available data, although observational data is relatively sparse on Svalbard. Section 4 describes the model results of the impact of sea ice decline on accumulation and melt climatology.

2 Model setup and methods

2.1 Model setup

A high resolution 25 km (0.22°) version of the UK Met Office RCM, HadRM3 was used for this study (Jones et al., 1995). The use of a high resolution model is necessary due to Svalbard's complex topography and will give significant improvement over lower resolution GCMs, typically of the order of 100–400 km, due to the RCMs ability to resolve circulation associated with small scale orographic features.

The climatological time slices of SSTs and sea ice that are used to force the RCM come from both observations and GCM simulations. These are monthly mean fields, averaged over a given interval and used to force the model periodically. The GCM scenarios used come from the UKMO HadGEM1 global climate model. These experiments were performed as part of the 3rd Climate Model Inter-comparison Project (CMIP3) and are available from the WCRP database (http://www-pcmdi.llnl.gov/ipcc/about_ipcc.php). This set of experiments contains a historical run for the 20th Century, forced with observed green house gas (GHG) concentrations (20C3M). Nakicenovic and Swart (2000), set out scenarios of 21st Century GHG emissions, of these we select A1B (severe) and A2 (less severe) to be used in this study. The source and time slice period of the SSTs and sea ice used for each of the 5 experiments are as follows:

1. ISST: Driven by U.K. Met Office Hadley Centre (MOHC) mean monthly observed SST and sea ice data (HadISST) for the period 1961–1990.

TCD
5, 1887–1920, 2011

2. 20C3M: present day control SST and sea ice (1961–1990),
3. A1B: A1B SST and sea ice (2061–2090),
4. A2: A2 SST and sea ice (2061–2090) and
5. HYB: A1B sea ice and 20C3M SSTs.

The ISST simulation will be used to compare RCM performance against observational data over Svalbard. Many studies use reanalysis products to force RCMs to isolate bias/errors in the RCM from those in the driving simulation (e.g. Noguer et al., 1998; Denis et al., 2002). The use of the HadISST observed SST and sea ice data set minimises errors in the surface boundary conditions as a source of bias in the RCM present day validation experiment (ISST) (Rayner et al., 2003).

For the hybrid forcing experiment, HYB, the RCM is forced with 20C3M SSTs and A1B sea ice. For grids cells which are ice covered in the 20C3M field but not in the equivalent A1B grid cell, their SST value is set to −1.8 °C. The comparison between this and the A1B experiment, forced with A1B SST and sea ice, allows us to isolate the component of the climate change signal which is attributed to sea ice alone from the coupled SST and sea ice signal simulated in the A1B experiment.

The RCM simulations were forced at their lateral boundary by the global AGCM HadAM3 (Pope et al., 2000). HadAM3 includes the same physics as HadRM3 and was forced with the same SSTs and sea ice as the high resolution model.

The ratio between the resolution of lateral boundary forcing used to force an RCM and the RCMs resolution, is usually between 2 and 5, with a maximum of 10 (Denis et al., 2002). When this ratio is too large, multiple nesting is sometimes used, this is where the global model is used to force an intermediate resolution RCM, which is in turn used to force the high resolution RCM (e.g. Christensen et al., 1998). Such a nesting "cascade" was used in this study since the ratio between the resolution of HadAM3 (2.5° × 3.75°) and HadRM3 (0.22°) is greater than 10. For this purpose a 0.44°HadRM3 simulation on a domain containing the high resolution domain was used to output boundary conditions for the 0.22° Svalbard domain.

TCD
5, 1887–1920, 2011

2.2 Methods

In Sect. 4.2 we use SMB seasonal sensitivity characteristics (SSCs) to look at the impact of sea ice decline on the mass balance of the glaciers and ice caps on Svalbard (Oerlemans and Reichert, 2000; Oerlemans et al., 2005). These SSCs are a 2×12 matrix giving the sensitivities of the mean net specific surface mass balance ($\bar{b}_n$) of a glacier to a change in temperature and precipitation in a given month (see Fig. 2). These were calculated using an energy balance model, described in Van de Wal and Oerlemans (1994), and perturbing the temperature and precipitation input.

The difference between the mean specific balance of a glacier surface in a perturbed climate, $\bar{b}_n$, may be expressed as:

$$\Delta\bar{b}_n = \bar{b}_n - \bar{b}_{n,\mathrm{ref}}, \tag{1}$$

where $\bar{b}_{n,\mathrm{ref}}$ is the glaciers specific balance in a reference (control) climatology. This may be expressed in terms of monthly mean precipitation P_k and temperature T_k as:

$$\Delta\bar{b}_n = \sum_{k=1}^{12} \left\{ S_{T,k}(T'_k - \theta) + S_{P,k}(P'_k - \zeta) \right\}, \tag{2}$$

where the sensitivity of mean surface mass balance to temperature is defined as:

$$S_{T,k} = \frac{\partial\bar{b}_n}{\partial T'_k}, \tag{3}$$

where T'_k is the temperature perturbation from the control climate for month k. The SSC of precipitation is defined similarly by:

$$S_{P,k} = \frac{\partial\bar{b}_n}{\partial P'_k}, \tag{4}$$

TCD
5, 1887–1920, 2011

where the precipitation perturbation P'_k from the control climate, at a given month k is defined as:

$$P'_k = \frac{P_k - P_{k,\mathrm{ref}}}{P_{k,\mathrm{ref}}}, \tag{5}$$

where P_k is the mean precipitation in the perturbed climate for month k and $P_{k,\mathrm{ref}}$ is the mean monthly precipitation in the reference. The terms θ and ζ are introduced to account for the imbalance between climate and glacier state. It is difficult to quantify these terms in the light of existing information about both the current state of the mass balance of Svalbard's glaciers and climatic conditions in the region. Hence we follow Oerlemans et al. (2005) in setting these to zero.

The use of these SSCs to relate climatic changes to changes in SMB requires the assumption that changes in SMB are linear with changes in temperature and precipitation. As such the calculated SMB anomaly from a given climatic perturbation is subject to large uncertainty. In this context, changes in $\bar{b}_n$ are best looked at as being indicative of relative changes in SMB between the simulations.

3 Comparison of model with observations

There are relatively few long-term meteorological station records in Svalbard, and even fewer records of any length from glaciated areas. Accordingly we also use some proxy data for validation purposes.

3.1 Comparison with meteorological station temperature

There are two long-term meteorological records available from Svalbard: Ny-Ålesund and Longyearbyen both in west Spitsbergen. A homogenised meteorological record for Longyearbyen is available from 1911-present, and is one of only a few long term temperature records in the Arctic (Nordli and Kohler, 2004). The temperature record

TCD
5, 1887–1920, 2011

from the research base in Ny-Ålesund, which is a coastal site, covers the period 1974-present.

Two glaciers with AWS station data available are Midre Lovénbreen and Kongsvegen, both near Ny-Ålesund, western Spitsbergen (see Fig. 1). The Midtre Lovénbreen record lasts from 1997–2002 (Hodson et al., 2005). Monthly mean values were calculated from the hourly met station temperatures. Despite the high resolution of the RCM, a single grid cell contains both the Midtre Lovénbreen station and Ny-Ålesund.

The Kongsvegen AWS is located at stake 6 (~530 m a.s.l., 78.78° N, 13.16° E), with a record covering the period 2000–2007.

For comparison with the RCM, a mean monthly temperature climatology was calculated from the available daily data at each site. In the case of Longyearbyen, where the record spans the reference period (1961–1990), only data from these years was used. For the other locations, where records are shorter, the whole period of available observations was used.

The RCM reproduces the summer temperature well in Midtre Lovénbreen and Ny-Ålesund, but is colder in winter at both these locations. This cold bias at these locations is probably caused by unrealistic levels of orographic blocking due to insufficiently resolved orography. Comparison with ERA-40 surface winds reveals an over dominance of cold katabatic easterly winds from Svalbard's interior. Even at 25 km there is a large step change in orographic height at the coast, blocking warm air from penetrating suitably far inland. The seasonal cycle of temperature at both these locations follows the nearest ocean cell in the RCM better than the containing land cell (see Fig. 3a). This indicates that easterly winds are overly dominant in winter in the model.

The RCM performs better at Longyearbyen, where the winter cold bias is about half that in Ny-Ålesund. In Longyearbyen, there is a smaller and more gradual increase in elevation from the western coast, such that the topography in the RCM is more representative of the meteorological station at Longyearbyen, which is close to sea level (see Fig. 2 and Fig. 3b).

TCD
5, 1887–1920, 2011

The RCM represents the annual temperature well at Kongsvegen but overestimates the seasonal variability, with too cold winter and too warm summer temperatures (see Fig. 3c). A similar pattern in HadRM3 was seen by Murphy et al. (2002) for locations on the Greenland ice sheet, which was associated with errors in the RCMs surface exchange scheme MOSES due to an oversimplification of the albedo scheme over ice.

This highlights the issues surrounding the comparison of point data with grid cell model data (Skelly and Henderson-Sellers, 1996). The often assumed equivalence between the two becomes less realistic as the level of real surface inhomogeneity increases. Svalbard is particularly inhomogeneous at the sub-25 km grid scale, and therefore one would expect there to be deviations from point observational data.

3.2 Melt climatology

With so few meteorological records available for comparison, and these restricted to the western coast of Svalbard, we look to the annual number of positive degree days (PDDs) as an alternative. A 5 year climatology of melt days was compiled for Svalbard for the period 2000–2004 by Sharp and Wang (2009) from backscatter data from the Quick Scatterometer (QSCAT). We use this as a climatology against which to validate model temperature. To do this we assume an equivalence of melt days and surface air temperature PDDs. This assumed equivalence is justified in that, to a first approximation, when the surface air temperature is positive the surface will be melting, and when the surface air temperature is negative it will not. The 1961–1990 observed mean SSTs and sea ice used to force the RCM are not equivalent to 2000–2004 SSTs and sea ice. However the lack of quality gridded temperature observations requires us to use alternative validation datasets such as this.

The RCM models the onset of melt well in south and west Spitsbergen but melt starts too early in east Spitsbergen and on Nordaustlandet. Similarly, melt season duration is modelled well in southern and eastern Spitsbergen, but the melt season is too short in north east Spitsbergen and Nordaustlandet (Fig. 4). This indicates that the RCM is too cold in these regions, which is likely caused by the same cold bias experienced in western Spitsbergen.

TCD
5, 1887–1920, 2011

The date of freeze onset is modelled well by the RCM in southern and eastern Spitsbergen, but the onset of melt is up to 25 days earlier in the RCM over Austfonna and ~10 days in Vestfonna and northeastern Spitsbergen. This is perhaps not due to deficiencies in the model but to differences in sea ice and SST between 2000–2004 and those used to force the RCM. In the 2000–2004 period the pack ice envelops northern Svalbard later in the season compared to the 1961–1990 baseline climatology used to force the RCM.

3.3 Accumulation validation

Direct observations of precipitation are problematic in cold regions, with rime ice or undercatch causing serious hindrance to accurate measurements (Førland and Hanssen-Bauer, 2003). However, ice cores can provide a record of specific net SMB, through analysis of annual layers or the dating of layers using reference horizons from e.g. volcanic eruptions (e.g. Banta and McConnell, 2007).

Pinglot et al. (1999) derived mean, minimum and maximum specific net SMB, b_n, records for a number of glaciers around Svalbard. Accumulation values were determined by dating layers using fallout from nuclear tests (1963) and the Chernobyl layer (1986) as temporal markers in the record. We use the ice core derived specific net SMB to compare against RCM precipitation in the grid cells containing these core sites (see Tables 1, 2 and Fig. 5a). Since these ice core sites are in the accumulation zone of their respective glacier, annual accumulation forms a lower bound to total precipitation. The less melt occurring at the ice core site the better an approximation of total precipitation b_n becomes. This allows us to determine those grid cells that underestimate precipitation.

Analysis reveals that the RCM has ample precipitation over all ice core locations in Spitsbergen but underestimates precipitation at both sites on Nordaustlandet (Fig. 5b). The RCM underestimates the accumulation at the Aust 98 and Vest 95 sites producing 18 % and 62 % of that observed respectively (see Table 2). This may be caused by a mixture of the RCM underestimating orographic precipitation due to low elevations

TCD
5, 1887–1920, 2011

in the RCM relative to reality and the block like nature of the Nordaustlandet coastline which has a much steeper gradient than in reality (Fig. 5c). The cold bias mentioned will reduce accumulation rates by causing a reduction in specific humidity in north Svalbard. However, the accumulation rates on Svalbard are extremely variable both spatially and temporally with accumulation experiencing large inter-annual variation (Sand et al., 2003). Understanding of these processes is limited by a lack of available observational data on Nordaustlandet.

4 The impact of changes in sea ice to the climate of Svalbard

The previous section showed that although the model is not perfect, it does successfully represent many details of Svalbard's climate relevant to the SMB. In this section we will present the impacts of the driving scenarios, firstly on the surface energy balance of the Arctic Ocean surrounding Svalbard and their impact on Svalbard's climatic regime. Secondly, we describe the impact of the climatic perturbations to the SMB of Svalbard's glaciers and ice caps.

4.1 Energy balance, hydrological cycle and temperature

The area of greatest projected sea ice retreat in the east Arctic is around Svalbard (Fig. 6). Svalbard is intersected by the March sea ice maximum extent for the 20C3M present day experiment and sea ice covers much of the Barents sea. In all future scenarios the southern March maximum extent has migrated north past the 80° latitude band leaving open water to both the north and eastern shores of Svalbard (Fig. 7).

During the September minimum of the 20C3M climate, the sea ice edge reaches the northeastern coast of the Svalbard archipelago. In the future scenarios the Arctic is almost completely ice-free, other than some small protected areas around the north coast of Greenland and the Canadian archipelago.

TCD
5, 1887–1920, 2011

In all three future simulations, there are large increases in surface turbulent heat flux (THF) over areas experiencing a reduction in sea ice concentration. This is most pronounced in DJF, since the atmosphere is coldest relative to the ocean in this season. There is a pronounced dipole pattern in the DJF THF anomaly, with positive anomalies between the 20C3M and future sea ice edge and negative anomalies south of the 20C3M sea ice edge. The area south of the sea ice edge is a maxima of THF field, since the open ocean is in contact with extremely cold polar air (Fig. 6). In a reduced sea ice scenario, this maxima occurs just to the south of the future sea ice edge, this effect was also observed in the study of Deser et al. (2010).

The sea ice edge in the 20C3M DJF climatology lies close to Svalbard, such that in reduced sea ice scenarios the ocean to the southwest experiences less THF, while the water around the northeastern coast experiences a much increased THF. The areas of largest increase are in the Barents and Kara Sea, where winter anomalies are over 110 Wm^{-2} in places (Fig. 6).

Both A1B and A2 show large DJF temperature anomalies, with temperatures increasing by as much as 21 °C in north east Nordaustlandet. There is a large gradient of change between the west coast of Spitsbergen and Nordaustlandet, with the west coast experiencing more moderate changes of 8 °C. The decline of sea ice around the eastern side of the archipelago amplifies warming in this region. Changes are more moderate in HYB as one might expect, with changes of 0–15 °C between the west and east coast (see Table 3 and Fig. 6). This is the portion of the change which is due to the impact of sea ice declining in this region. Indicating that sea ice decline alone is responsible for roughly ~66 % of the DJF warming in the A1B scenario.

The resulting changes to DJF precipitation are also dramatic, with A1B and A2 showing precipitation anomalies of more than 400 % over Nordastlandet (Fig. 6 and Table 3). These changes are the result of an altered hydrological cycle in the region, due to the previously described changes in THF as well as changes in circulation, with the winter prevailing wind direction changing from predominantly northwest to southwest (not shown). This southerly shift in wind direction over Svalbard is caused by the change in

TCD
5, 1887–1920, 2011

thermal gradient over the Barents and Kara Seas.

Large increases in precipitation are observed over the entire Nordaustlandet, and in northeastern Spitsbergen. However parts of western Spitsbergen experience less change, and some coastal locations near Isfjorden even experience a small reduction in precipitation. Whilst warmer temperatures in the region mean that there is more moisture transport and precipitation over the archipelago, the negative THF anomalies in the Greenland sea to the west coast of Spitsbergen cause this decrease in precipitation in parts of the east coast.

The relatively low prevailing wind speeds in the Arctic mean that the anomalies of precipitation for both DJF and JJA closely follow the anomalies of THF, especially in the HYB experiment. The precipitation anomaly caused by sea ice decline in HYB has a clear dipole pattern with areas of increased THF having increased precipitation and negative THF areas reduced precipitation (Fig. 6).

Svalbard experiences a more moderate increase in DJF precipitation of ~54% in HYB but with a similar spatial pattern to A1B and A2 experiments. There are small negative changes around west Spitsbergen and large changes (~270 %) over Nordaustlandet. The changes in precipitation in HYB are the result of changes in THF alone, thus the impacts of sea ice decline which are of a fairly local nature are separated from the impacts of increased global SSTs. Thus, those changes in precipitation due to large scale moisture transport anomalies are excluded.

Though the reduction in sea ice extent over the Arctic is greater in JJA than DJF the reduction in sea ice concentration over the Barents sea in JJA is less than in DJF, this is because in 20C3M the Barents sea has lower concentrations than in the winter, when most grids are 100 % covered. Thus the areas which experience the largest reduction in sea ice between the 20C3M and future climates are north of Svalbard and Franz Joseph Land (Fig. 8).

The HYB experiment's JJA THF response due to sea ice reduction alone is small and negative over some areas where ice is removed. This is because the SST for these cells was set to −1.8 °C which is colder than the atmosphere (see HYB in Fig. 8).

TCD
5, 1887–1920, 2011

There is no change in SST or surface air temperature, hence no change in thermal gradient. However the response to sea ice and SSTs in A1B and A2 experiments is more noticeable with a positive response everywhere between the 20C3M maximum ice extent line and the maximum ice extent line in the future simulations. The area with the largest positive response is off the north and south coasts of Svalbard.

The JJA temperature response in the HYB experiment is small with some isolated decreases in temperature. The A1B and A2 temperature responses are more significant, with positive anomalies of 0–5 °C, with changes located mainly in southern Spitsbergen and Edgeøya.

Similarly, the JJA changes to precipitation are relatively small in HYB (−30–40 % in some areas) with positive changes in the north and negative changes in some southern and central areas. When SST changes are included, some areas experience over 100 % increases with the largest changes occurring in northeastern Spitsbergen and Nordaustlandet. More moderate increases occur on the west coast of Spitsbergen. This is driven by both increased turbulent heat flux from the Arctic Ocean and poleward moisture transport from lower latitudes.

The changes in temperature and precipitation for the Barents sea region described in this section are more dramatic than the estimates of Førland et al. (2009) but similar to those of Rinke and Dethloff (2008). This provides some confidence in the magnitude of simulated change. The seasonal dependance of changes in precipitation and temperature are similar to both these studies. However, it should be noted that the periods of analysis and scenarios are not consistent between these experiments.

4.2 Surface mass balance

In this section the impact of those climatic changes described in Sect. 4.1 to the surface mass balance (SMB) of Svalbard's glaciers and ice caps will be described.

For each experiment, A1B, A2 and HYB, the change in specific balance, $\Delta\bar{b}_n$, across all the ice masses across the archipelago was calculated based on the SSCs of Oerlemans et al. (2005) (Fig. 1). They were calculated using Eq. (2) where the changes

TCD
5, 1887–1920, 2011

in precipitation and temperature were area averaged across the whole of Svalbard and the reference climate was the 20C3M experiment. For A1B, A2 and HYB the values of $\Delta\bar{b}_n$ are −0.31, −0.31 and 0.35 m water equivalent (w.e.) respectively.

In the A1B and A2 experiments the $\Delta\bar{b}_n$ is dominated by negative mass balances resulting from increases in the melt season temperature (Fig. 9a). Accumulation increases throughout the year, especially in winter months, but while it compensates the melt driven mass loss to some extent, the increase is not enough to avoid a negative $\Delta\bar{b}_n$ (Fig. 9b). In reality an increase in summer liquid precipitation would act as a heat gain to the surface and causes melt, an effect that is not accounted for by the SSCs and one that would result in an even more negative change in $\bar{b}_n$, in both A1B and A2 experiments.

The HYB experiment however experiences a net increase in $\bar{b}_n$, which is caused by both a decrease in melt season temperature discussed in Sect. 4 causing less melt and an increase in DJF accumulation (Fig. 9b). There is a decrease in accumulation in JJA but Svalbard is not sensitive to changes in accumulation during the melt season and this is more than compensated by increases in accumulation in DJF. Significant increases in temperature occur outside of the present day melt season between September–May; these do not affect the calculated change in $\bar{b}_n$ since the values of $S_{T,k}$ is zero in these months, but this will not be the case if temperatures rise above 0 °C.

The fact that the temperature and precipitation response in A1B and A2 is similar to Rinke and Dethloff (2008) and the THF response in HYB similar to Deser et al. (2010) is encouraging and provides confidence in the robustness of these results.

5 Conclusions

5.1 Model validation

The use of high resolution regional models in areas of complex topography like Svalbard is essential to understanding future cryospheric change. In this study it has been

TCD
5, 1887–1920, 2011

demonstrated that the 25 km (0.22°) version of HadRM3 performs well in reproducing some aspects of Svalbard's climate in the present day. The model was validated against in-situ meteorological station data from the Norsk Polarinstitutt research station at Ny-Ålesund and AWS data from the near by glaciers Midtre Lovénbreen and Kongsvegen as well data for Longyearbyen airport near Isfjorden.

The RCM performed well in JJA but was affected by excessive blocking of coastal air masses, leading to an over dominance of cold air from the north and large winter biases. The performance of HadRM3 suggests that even at 25 km resolution the orography was not suitably resolved to model circulation at the coastal locations well enough to generate accurate surface fields for forcing a more complicated SMB model. Future climate modelling studies of this region would benefit from the use of even higher resolution models.

Model precipitation was validated against in-situ observations of net accumulation derived from ice cores (Pinglot et al., 1999). The model reproduced precipitation well at all of the sites on Spitsbergen but under represented precipitation at sites on Nordaustlandet. These low precipitation rates were attributed to lower orographic elevation thus less orographic precipitation than reality.

The use of the melt season climatology of Sharp and Wang (2009) as a means to validate the RCM is unusual but utilises an equivalence with PDDs that makes sense physically. We decided against regridding the data onto the same grid as the RCM or vice versa and performing more robust statistical tests since the two quantities are not equivalent. The differences in climate state between both the modelled period and period of observation also inhibit a fair comparison of these quantities. Nonetheless in regions of sparse observations, the data provides some qualitative assessment which is useful.

5.2 Climate change and mass balance

This study has investigated the impact of 21st Century sea ice decline on the mass balance of Svalbard's ice caps and glaciers by partitioning the signal of sea ice decline

TCD
5, 1887–1920, 2011

on Svalbard's climate from the coupled impact of SST increase and sea ice decline. In doing so we found that ~66 % of the DJF warming and ~54% of the increase in precipitation between 1961–1990 and the A1B 2061–2090 scenario was caused by the effect of sea ice decline. In contrast to DJF, where removing the sea ice cover had a large impact, in JJA changes in SST are responsible for changes in THF. In JJA the sea ice decline alone causes relatively little change in temperature nor precipitation over Svalbard compared to the DJF anomalies. However when changes in SST are also included, the net effect in the A1B simulation is a significant increase in both precipitation and temperature.

Sea ice decline alone causes a net increase in the mass balance of Svalbard's glaciers. The HYB experiment shows a decrease in summer temperatures and an increase in annual precipitation leading to a positive net change in specific SMB averaged across the archipelago of 0.35 m w.e. This is in stark contrast to the coupled effect in the A1B simulation which shows a net decrease in SMB −0.31 m w.e. Both these changes are similar in magnitude to the present day mass balance for Svalbard ($=-0.36\,\mathrm{m\,a^{-1}}$ w.e., excluding Austfonna and Kvitøya) (Nuth et al., 2010).

The magnitude of change in the A1B and A2 scenarios is similar due to similar SST and sea ice extent forcing over the period used. This is because, at this stage in the evolution of these different emission scenarios, the forcing is similar (Nakicenovic and Swart, 2000). This increases the robustness of the magnitude of change simulated for this period.

The method of using SSC to assess the change in mass balance has been used to look at the long term impacts of climate change (Oerlemans et al., 2005). This assumes that $\bar{b}_n$ changes linearly with temperature and precipitation change. A more physically based SMB impact study using an energy balance model would be a more robust approach to modelling the impact of the changes modelled by the RCM, however the SSCs provide a first order approximation of change suitable for this study as we are more interested in the relative impact of changes in sea ice and SST.

TCD
5, 1887–1920, 2011

Acknowledgements. This work was carried out using the computational facilities of the Advanced Computing Research Centre, University of Bristol – http://www.bris.ac.uk/acrc/. Assistance in using HadRM3 was provided by the National Center for Atmospheric Science (NCAS). We acknowledge the modeling groups, the Program for Climate Model Diagnosis and Intercomparison (PCMDI) and the WCRP's Working Group on Coupled Modelling (WGCM) for their roles in making available the WCRP CMIP3 multi-model dataset. Support of this dataset is provided by the Office of Science, U.S. Department of Energy.

References

Arendt, A. A., Echelmeyer, K. A., Harrison, W. D., Lingle, C. S., and Valentine, V. B.: Rapid Wastage of Alaskan Glaciers and their Contribution to Rising Sea Level, Science, 297, 382–386, 2002. 1888

Bamber, J., Krabill, W., Raper, V., and Dowdeswell, J.: Anomalous recent growth of part of a large Arctic ice cap: Austfonna, Svalbard, Geophys. Res. Lett., 31, L12402, 4 pp., doi:10.1029/2004GL019667, 2004. 1889

Banta, J. R. and McConnell, J. R.: Annual accumulation over recent centuries at four sites in central Greenland, J. Geophys. Res.-Atmos., 112, D10114, 9 pp., doi:10.1029/2006JD007887, 2007. 1897

Benestad, R. E., Førland, E. J., and Hanssen-Bauer, I.: Empirically downscaled temperature scenarios for Svalbard, Atmos. Sci. Lett., 3, 71–93, doi:10.1006/asle.2002.0050, 2002. 1890

Boé, J. L., Hall, A., and Qu, X.: September sea-ice cover in the Arctic Ocean projected to vanish by 2100, Nat. Geosci., 2, 341–343, 2009. 1889

Christensen, O. B., Christensen, J. H., Machenhauer, B., and Botzet, M.: Very high-resolution regional climate simulations over Scandinavia - Present climate, J. Climate, 11, 3204–3229, 1998. 1892

Denis, B., Laprise, R., Caya, D., and Cote, J.: Downscaling ability of one-way nested regional climate models: the Big-Brother Experiment, Clim. Dynam., 18, 627–646, 2002. 1892

Deser, C., Tomas, R., Alexander, M., and Lawrence, D.: The Seasonal Atmospheric Response to Projected Arctic Sea Ice Loss in the Late Twenty-First Century, J. Climate, 23, 333–351, 2010. 1889, 1899, 1902

TCD

5, 1887–1920, 2011

Divine, D. V. and Dick, C.: Historical variability of sea ice edge position in the Nordic Seas, J. Geophys. Res.-Ocean, 111, C01001, 14 pp., doi:10.1029/2004JC002851, 2006. 1889
Dyurgerov, M., Bring, A., and Destouni, G.: Integrated assessment of changes in freshwater inflow to the Arctic Ocean, J. Geophys. Res.-Atmos., 115, D12116, 9 pp., doi:10.1029/2009JD013060, 2010. 1888
Førland, E. J. and Hanssen-Bauer, I.: Climate variations and implications for precipitation types in the Norwegian Arctic, 24/02 klima, met.no, 2003. 1897
Førland, E. J., Benestad, R. E., Flatøy, F., Hanssen-Bauer, I., Haugen, J. E., Isaksen, K., Sorteberg, A., and Ådlaandsvic, B.: Climate development in North Norway and the Svalbard region during 1900–2100, 2009. 1890, 1901
Fowler, H., Blenkinsop, S., and Tebaldi, C.: Linking climate change modelling to impacts studies: recent advances in downscaling techniques for hydrological modelling, Int. J. Climatol., 27, 1547–1578, 2007. 1890
Hanssen-Bauer, I. and Førland, E.: Verification and analysis of a climate simulation of temperature and pressure fields over Norway and Svalbard, Clim. Res., 16, 225–235, 2001. 1890
Hodson, A. J., Kohler, J., Brinkhaus, M., and Wynn, P.: Multi-year water and surface energy budget of a high-latitude polythermal glacier: evidence for overwinter water storage in a dynamic subglacial reservoir, Ann. Glaciol., 42, 42–46, 2005. 1895
Isaksson, E., Divine, D., Kohler, J., Martma, T., Pohjola, V., Motoyama, H., and Watanabe, O.: Climate oscillations as recorded in Svalbard ice core delta O-18 records between AD 1200 and 1997, Geogr. Ann. A., 87A, 203–214, 2005a. 1889
Isaksson, E., Kohler, J., Pohjola, V., Moore, J., Igarashi, M., Karlf, L., Martma, T., Meijer, H., Motoyama, H., Vaikme, R., and van de Wal, R. S. W.: Two ice-core 18O records from Svalbard illustrating climate and sea-ice variability over the last 400 years, The Holocene, 15, 501–509, 2005b. 1889
Jones, R. G., Murphy, J. M., and Noguer, M.: Simulation of Climate-Change over Europe Using a Nested Regional-Climate Model .1. Assessment of Control Climate, Including Sensitivity to Location of Lateral Boundaries, Quarterly Journal of the Royal Meteorological Society, 121, 1413–1449, 1995. 1891
Kaser, G., Cogley, J. G., Dyurgerov, M. B., Meier, M. F., and Ohmura, A.: Mass Balance of Glaciers and Ice Caps: Consensus Estimates for 1961–2004, Geophys. Res. Lett., 33, L19501, 5 pp., doi:10.1029/2006GL027511, 2006. 1888

TCD
5, 1887–1920, 2011

Meier, M. F., Dyurgerov, M. B., Rick, U. K., O'Neel, S., Pfeffer, W. T., Anderson, R. S., Anderson, S. P., and Glazovsky, A. F.: Glaciers dominate Eustatic sea-level rise in the 21st century, Science, 317, 1064–1067, 2007. 1888

Moholdt, G., Nuth, C., Hagen, J. O., and Kohler, J.: Recent elevation changes of Svalbard glaciers derived from ICESat laser altimetry, Remote Sens. Environ., 114, 11, 2756–2767, doi:10.1016/j.rse.2010.06.008 2010. 1888

Murphy, B. F., Marsiat, I., and Valdes, P.: Atmospheric contributions to the surface mass balance of Greenland in the HadAM3 atmospheric model, J. Geophys. Res.-Atmos., 107(D21), 4556, 22 pp., doi:10.1029/2001JD000389, 2002. 1896

Nakicenovic, N. and Swart, R.: Special Report on Emissions Scenarios, Cambridge University Press, U.K., 612 pp., 2000. 1890, 1891, 1904

Noguer, M., Jones, R., and Murphy, J.: Sources of systematic errors in the climatology of a regional climate model over Europe, Clim. Dynam., 14, 691–712, 1998. 1892

Nordli, ø. and Kohler, J.: The early 20th century warming. Daily observations at Grnfjorden and Longyearbyen on Spitsbergen, Tech. Rep. 12/03, DNMI/klima, 2004. 1889, 1894

Nuth, C., Moholdt, G., Kohler, J., Hagen, J. O., and Kb, A.: Svalbard glacier elevation changes and contribution to sea level rise, J. Geophys. Res., 115, F01008, 16 pp., doi:10.1029/2008JF001223, 2010. 1888, 1904

Oerlemans, J. and Reichert, B.: Relating glacier mass balance to meteorological data by using a seasonal sensitivity characteristic, J. Glaciol., 46, 1–6, 2000. 1893

Oerlemans, J., Bassford, R. P., Chapman, W., Dowdeswell, J. A., Glazovsky, A. F., Hagen, J. O., Melvold, K., de Wildt, M. D., and van de Wal, R. S. W.: Estimating the contribution of Arctic glaciers to sea-level change in the next 100 years, Ann. Glaciol., 42, 230–236, 2005. 1893, 1894, 1901, 1904, 1913

Pinglot, J. F., Pourchet, M., Lefauconnier, B., Hagen, J. O., Isaksson, E., Vaikmae, R., and Kamiyama, K.: Accumulation in Svalbard glaciers deduced from ice cores with nuclear tests and Chernobyl reference layers, Polar Res., 18, 315–321, 1999. 1897, 1903

Pope, V. D., Gallani, M. L., Rowntree, P. R., and Stratton, R. A.: The impact of new physical parametrizations in the Hadley Centre climate model: HadAM3, Clim. Dynam., 16, 123–146, 2000. 1892

Raper, V., Bamber, J., and Krabill, W.: Interpretation of the anomalous growth of Austfonna, Svalbard, a large Arctic ice cap, Ann. Glaciol., 42, 373–379, 2005. 1889

Rayner, N. A., Parker, D. E., Horton, E. B., Folland, C. K., Alexander, L. V., Rowell, D. P., Kent,

TCD
5, 1887–1920, 2011

E. C., and Kaplan, A.: Global analyses of sea surface temperature, sea ice, and night marine air temperature since the late nineteenth century, J. Geophys. Res.-Atmos., 108(D14), 4407, 29 pp., doi:10.1029/2002JD002670 2003. 1892
Rinke, A. and Dethloff, K.: Simulated circum-Arctic climate changes by the end of the 21st century, Global Planet. Change, 62, 173–186, 2008. 1901, 1902
Rye, C. J., Arnold, N. S., Willis, I. C., and Kohler, J.: Modeling the surface mass balance of a high Arctic glacier using the ERA-40 reanalysis, J. Geophys. Res.-Earth, 115, F02014, 18 pp., doi:10.1029/2009JF001364, 2010. 1890
Sand, K., Winther, J. G., Marechal, D., Bruland, O., and Melvold, K.: Regional variations of snow accumulation on Spitsbergen, Svalbard, 1997–99, Nordic Hydrology, 34, 17–32, 2003. 1898
Serreze, M., Holland, M. M., and Stroeve, J.: Perspectives on the Arctic's Shrinking Sea-Ice Cover, Science, 315, 2007. 1889
Serreze, M. C., Barrett, A. P., Stroeve, J. C., Kindig, D. N., and Holland, M. M.: The emergence of surface-based Arctic amplification, Cryosphere, 3, 11–19, 2009. 1889
Sharp, M. and Wang, L. B.: A Five-Year Record of Summer Melt on Eurasian Arctic Ice Caps, J. Climate, 22, 133–145, 2009. 1896, 1903
Singarayer, J. S., Bamber, J. L., and Valdes, P. J.: Twenty-first-century climate impacts from a declining Arctic sea ice cover, J. Climate, 19, 1109–1125, 2006. 1889
Skelly, W. C. and Henderson-Sellers, A.: Grid Box or Grid Point: what type of data do GCMs deliver to Climate Impacts Researchers?, Int. J. Climatol., 16, 1079–1086, 1996. 1896
Stein, U. and Alpert, P.: Factor separation in numerical simulations, J. Atmos. Sci., 50, 2107–2115, 1993. 1889
Stroeve, J., Holland, M. M., Meier, W., Scambos, T., and Serreze, M.: Arctic sea ice decline: Faster than forecast, Geophys. Res. Lett., 34, L09501, 5 pp., doi:10.1029/2007GL029703, 2007. 1889
Van de Wal, R. S. W. and Oerlemans, J.: An energy-balance model for the Greenland ice-sheet, Global Planet. Change, 9, 115–131, 1994. 1893
Wang, M. Y. and Overland, J. E.: A sea ice free summer Arctic within 30 years?, Geophys. Res. Lett., 36, L07502, 5 pp., doi:10.1029/2009GL0378202009. 1889
Wouters, B., Chambers, D., and Schrama, E. J. O.: GRACE observes small-scale mass loss in Greenland, Geophys. Res. Lett, 35, L20501, 5 pp., doi:10.1029/2008GL0348162008. 1888

TCD
5, 1887–1920, 2011

Table 1. Ice core name, location, altitude, equilibrium line altitude and the period the ice core covers for the ice core sites used in this study.

Glacier	Ice core	long	lat	Alt. (m)	ELA (m)	Period
Kongsvegen	Kong K	13.28	78.78	639	520	1963–1988
	Kong L	13.45	78.77	726	520	1965–1991
Snøfjella	Sno W	13.28	79.13	1190	650	1963–1991
Vestfonna	Vest 95	21.02	79.97	600	505	1963–1994
Austfonna	Aust 98	24.00	79.80	740	505	1963–1997
Lomonosovfonna	Lom 10	17.42	78.87	1230	660	1963–1996
Åsgårdfonna	Asg 93	16.72	79.45	1140	800	1963–1992

TCD
5, 1887–1920, 2011

Table 2. Specific net SMB average, minimum and maximum estimates from ice cores and RCM annual precipitation and standard deviation. The altitude of the ice core location and the RCM grid cell orographic height are included.

	Ice core				RCM			
		Balance (m w.e.)				Balance (m w.e.)		
Ice core	Alt.(m)	Ave.	Min.	Max.	Alt.(m)	Ave.	σ	diff. Ave.
Kong K	639	0.48	0.45	0.52	474	0.58	0.14	0.10
Kong L	726	0.60	0.56	0.64	474	0.58	0.14	−0.02
Sno W	1190	0.47	0.45	0.51	604	0.51	0.11	0.04
Vest 95	600	0.38	0.37	0.39	271	0.14	0.03	−0.24
Aust 98	740	0.50	0.50	0.51	502	0.41	0.07	−0.09
Lom 10	1230	0.36	0.35	0.37	725	0.34	0.05	−0.02
Asg 93	1140	0.31	0.30	0.33	538	0.44	0.06	0.13

TCD
5, 1887–1920, 2011

Table 3. Seasonal estimates of area averaged temperature and precipitation change on Svalbard for A1B, A2 and HYB simulations, compared to 20C3M control experiment. The intervals expresses the geographical spread of change, not projection uncertainty.

Field	Season	A1B	A2	HYB
Temperature (˚C)	ANN	5–12	6–12	0–6
	MAM	5–11	6–12	0–7
	JJA	0–5	0–5	−3–0
	SON	6–13	6–13	0–5
	DJF	8–21	8–21	0–15
Precipitation (%)	ANN	−9–232	−4–213	−14–101
	MAM	−19–264	−7–216	−20–148
	JJA	14–125	10–105	−29–38
	SON	−25–201	−21–233	−32–47
	DJF	−17–445	−10-446	−13–273

TCD
5, 1887–1920, 2011

Fig. 1. Map of the Svalbard archipelago including names of islands (Large font), locations (bold) and ice caps (italic).

TCD
5, 1887–1920, 2011

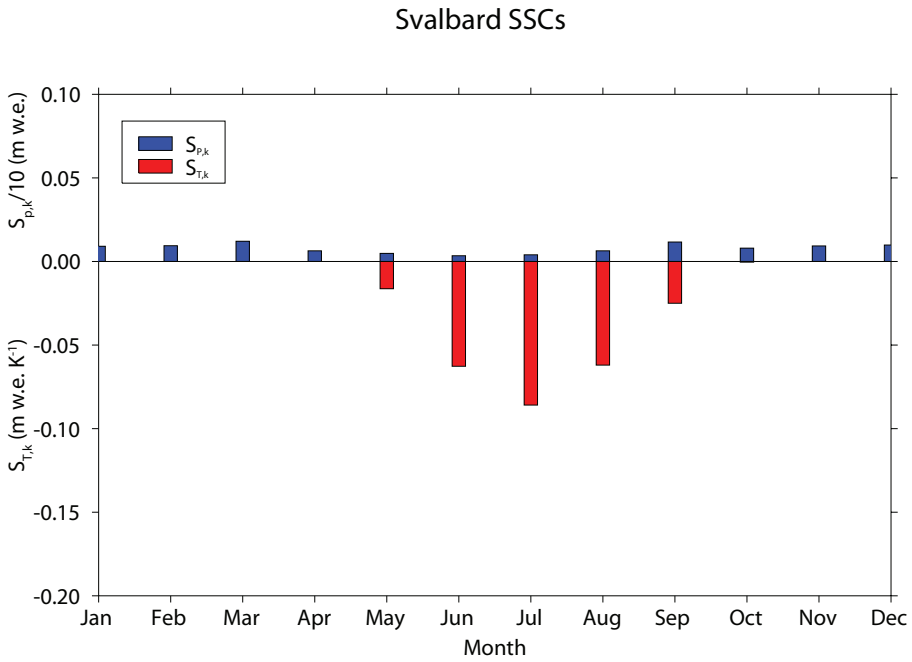

Fig. 2. Seasonal sensitivity characteristics (SSCs) for Svalbard from Oerlemans et al. (2005).

TCD
5, 1887–1920, 2011

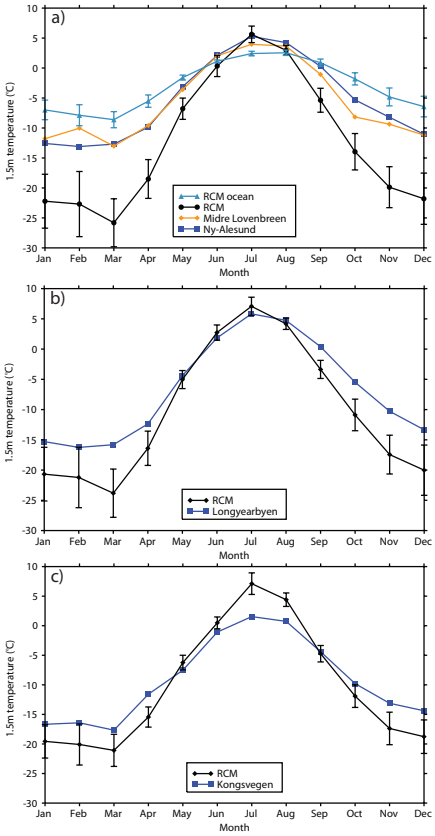

Fig. 3. Modelled and observed mean monthly surface air temperature for, the grid cell containing **(a)** Ny-Ålesund and Midtre Lovénbreen, **(b)** Longyearbyen and **(c)** Kongsvegen. In addition, temperature from the grid cell from the nearest ocean grid cell to Ny-Ålesund is plotted in **(a)** for comparison with the land cell. Each of the RCM mean monthly values have whiskers representing $\pm\sigma$.

TCD
5, 1887–1920, 2011

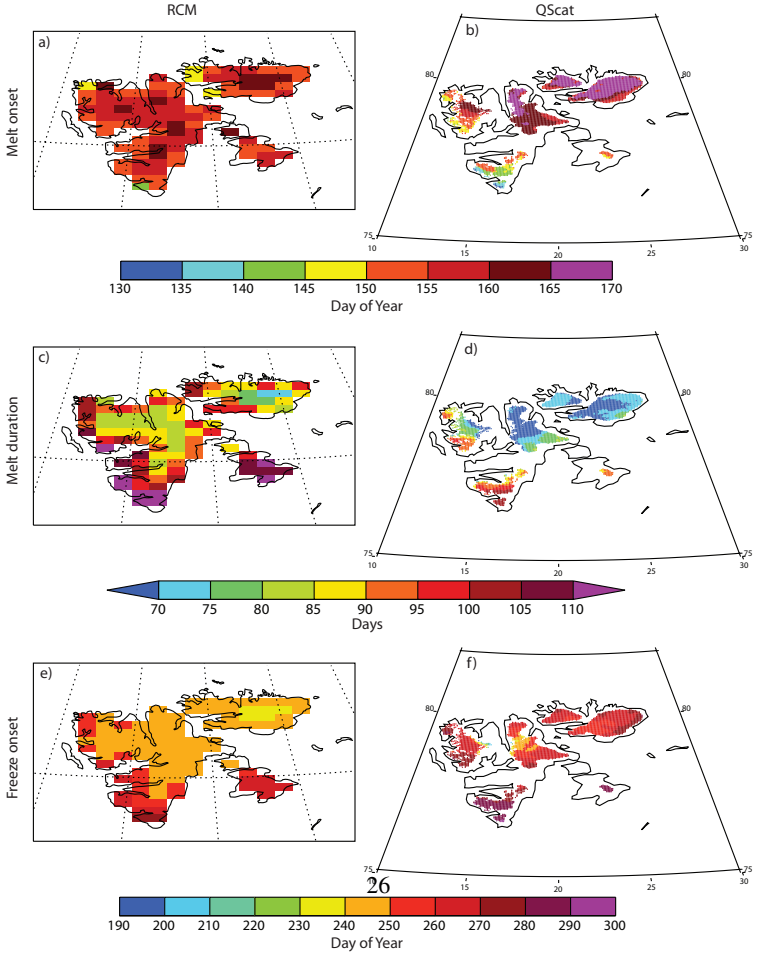

Fig. 4. Modelled and observed climatology of melt onset **(a** and **b)**, melt season duration **(c** and **d)** and freeze onset **(e** and **f)**.

TCD
5, 1887–1920, 2011

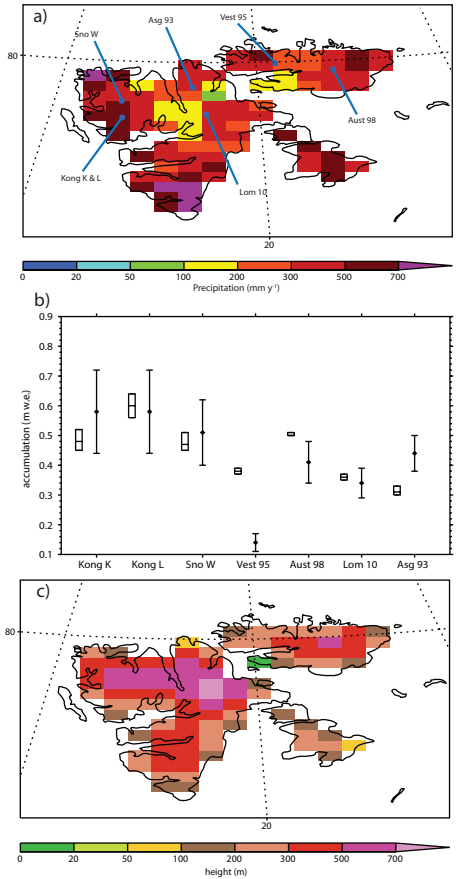

Fig. 5. annual total accumulation (precipitation) and ice corelocations (blue), **(a)**, Ice core net accumulation min, mean, max (box) and RCM total accumulation ($\pm\sigma$, whiskers), **(b)**, and RCM orographic height, **(c)** .

TCD
5, 1887–1920, 2011

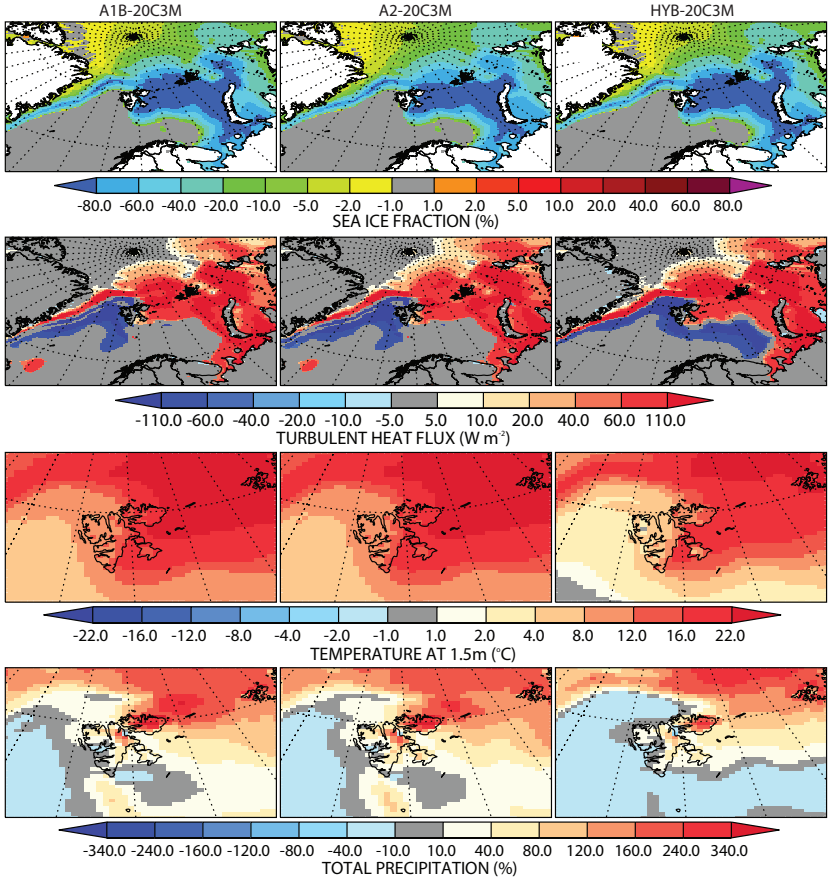

Fig. 6. DJF anomalies of sea ice concentration (%), turbulent heat flux ($W m^{-2}$), surface air temperature (°C) and precipitation (%) of the A1B, A2 and HYB from the 20C3M simulation.

TCD
5, 1887–1920, 2011

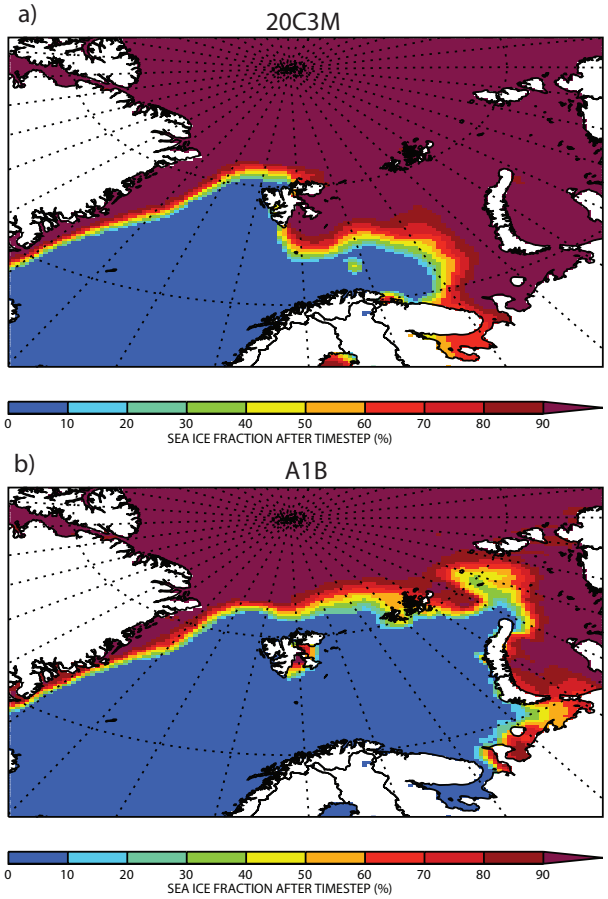

Fig. 7. March (maximum) mean sea ice concentration for **(a)**, 20C3M experiment and **(b)** A1B experiment. Derived from the HadGEM1 CMIP3 experiments.

TCD
5, 1887–1920, 2011

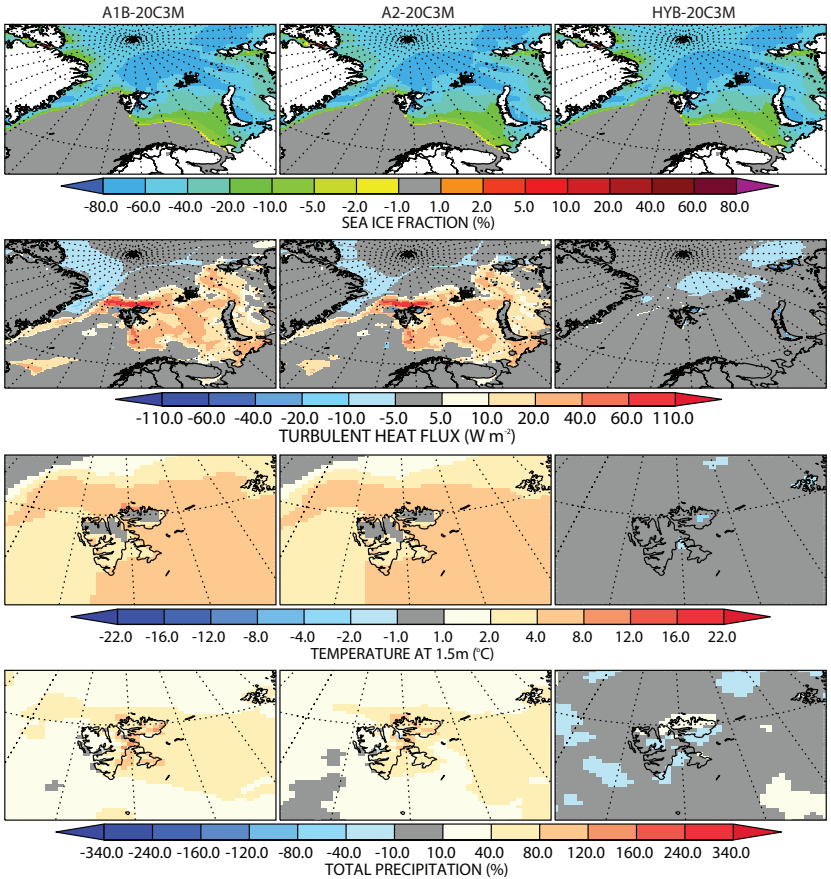

Fig. 8. JJA anomalies of sea ice concentration (%), turbulent heat flux ($W\,m^{-2}$), surface air temperature (°C) and precipitation (%) of the A1B, A2 and HYB from the 20C3M simulation.

TCD
5, 1887–1920, 2011

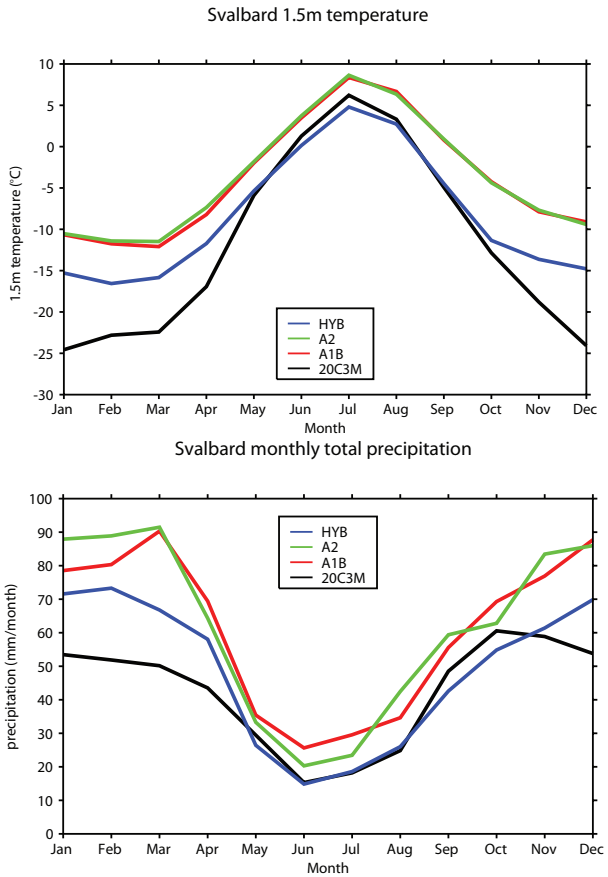

Fig. 9. Svalbard's monthly mean areal averaged cycle of surface air temperature (˚C), **(a)**, and precipitation (mm/month), **(b)**.

TCD
5, 1887–1920, 2011